iEMSs 2008:International Congress on Environmental Modelling and Software
Integrating Sciences and Information Technology for Environmental Assessment and Decision Making
4th Biennial Meeting of iEMSs, http://www.iemss.org/iemss2008/index.php?n=Main.Proceedings
M. Sànchez-Marrè, J. Béjar, J. Comas, A. Rizzoli and G. Guariso (Eds.)
International Environmental Modelling and Software Society (iEMSs), 2008

Implicit Large Eddy Simulation - a Promising Method for Turbulence Modelling in High Resolution Models

V. Fuka [a], **J. Brechler**[a]

[a]*Dept. of Meteorology and Env. Protection, Charles University, V Holešovičkách 2, Prague 8, 180 00, Czech Republic (vladimir.fuka@gmail.com, josef.brechler@mff.cuni.cz)*

Abstract: Implicit Large Eddy Simulation is an emerging tool for turbulence modelling. Instead of explicitely computing subgrid stress models, numerical dissipation of nonlinear schemes can be used as a main control mechanism of turbulent energy transfer. In this contribution we test performance of a high-resolution incompressible projection method in modelling of the Taylor-Green vortex flow, which stands as a prototype of a simple free flow with a transition to turbulence and a turbulence decay. Several criteria are used to asses the model, including the kinetic energy dissipation rate, kinetic energy spectra and probability density functions of velocity gradients.

Keywords: large eddy simulation; turbulence decay; turbulence simulation

1 INTRODUCTION

At the present time a new field of turbulence modelling called Implicit Large Eddy Simulation (ILES) (for a comprehensive review see Grinstein et al. [2007b]) enables turbulent flow computations with methods most commonly used for compressible fluid dynamics with shocks. These so called shock-capturing schemes can describe flows with very strong gradients using convection terms with nonlinear numerical diffusion. This numerical dissipation is stronger in areas with larger gradients and smaller in smooth parts. Nonlinearity can be achieved using explicit numerical diffusion terms (similar to traditional subgrid stress models) like Jameson et al. [1981] or implicitly using flux or slope limiters [Harten, 1983; van Leer, 1979]. Especially the second way proved to be efficient way of simulating compressible turbulent flows. Because of monotonicity preserving of these schemes, this kind of LES is also known as MILES - monotonically integrated large eddy simulation). To the most used methods belongs flux-corrected transport (FCT) [Boris and Book, 1997], PPM [Colella and Woodward, 1984] or MPDATA [Smolarkiewicz and Margolin, 1998]. MPDATA is used mainly for geophysical applications, which is also aim of our work.

Most of present ILES methods were developed in the framework of compressible flow solvers. Our aim is to develop and test similar method in traditional incompressible code. Schemes for incompressible flows mostly employ artificial compressibility method or projection methods. In artificial compressibility methods schemes for compressible fluid dynamics can be used in a straightforward way.

Projection methods, also known as fractional step methods [Brown et al., 2001], can be divided into two groups – exact projection methods and approximate projection methods. Approximate projection methods mostly employ cell centered grids and enable easier usage of high resolution methods [Almgren et al., 1996, 1998] at the cost of more difficult treatment of velocity – pressure coupling. Exact projection methods [Kim and Moin, 1985] provide very velocity – pressure coupling on staggered grids, but the usage of high resolution methods is complicated.

First example of an exact projection method on a staggered grid with high resolution advective scheme was a method by Tau [1994]. This scheme used a projection method of Bell et al. [1989] with Godunov method for advective fluxes modified for a staggered grid in 2D. This unique combination was emphasised by Rider [1998]. We choose this method as a base for our 3D model for incompressible implicit large eddy simulation.

As a first test case we computed Taylor-Green vortex flow, which serves as a simple example of free flow with transition to turbulence and subsequent turbulent decay. This flow was used for this purpose by several other authors, for example [Bensow et al., 2007; Garnier et al., 1999; Grinstein et al., 2007a]. The comparison is usually done with direct numerical simulation (DNS) data of Brachet et al. [1983] and Brachet [1991].

2 NUMERICAL METHOD

2.1 Projection methods

Our code solves the incompressible Navier-Stokes equations in the form

$$\frac{\partial u}{\partial t} + (\boldsymbol{u}\cdot\nabla)\boldsymbol{u} = -\nabla p + \nu\Delta\boldsymbol{u}, \tag{1}$$

$$\nabla\cdot\boldsymbol{u} = 0, \tag{2}$$

where $\boldsymbol{u} = (u, v, w)$ is the velocity vector, p is the pressure and ν is the coefficient of the kinematic viscosity.

The core of numerical method we used is a second order accurate projection method by Bell et al. [1989], adapted to 2D staggered grids by Tau [1994]. The main stages of one time step can be written as

$$\frac{\boldsymbol{u}^*_{i,j,k} - \boldsymbol{u}^n_{i,j,k}}{\Delta t} + \nabla_{i,j,k} p^{n-\frac{1}{2}} = -\left[(\boldsymbol{u}\cdot\nabla)\boldsymbol{u}^n\right]^{n+\frac{1}{2}}_{i,j,k} + \frac{\nu}{2}\left(\Delta_{i,j,k}\boldsymbol{u}^n + \Delta_{i,j,k}\boldsymbol{u}^*\right), \tag{3}$$

$$\tilde{\boldsymbol{u}}_{i,j,k} = \boldsymbol{u}^*_{i,j,k} + \nabla_{i,j,k} p^{n-\frac{1}{2}}, \tag{4}$$

$$\Delta_{i,j,k}\varphi = (\nabla\cdot)_{i,j,k}\tilde{\boldsymbol{u}}, \tag{5}$$

$$\boldsymbol{u}^{n+1}_{i,j,k} = \tilde{\boldsymbol{u}}_{i,j,k} - \Delta t\nabla_{i,j,k}\varphi, \tag{6}$$

$$p^{n+\frac{1}{2}}_{i,j,k} = \varphi_{i,j,k}, \tag{7}$$

where $\boldsymbol{u}^*$ does not obey the continuity equation and in the next stage is projected onto a solenoidal field using the so called pressure form of the exact projection. The diffusion terms are treated by means of the implicit Crank-Nicolson method in the equation (3).

2.2 High-resolution advection method

The advection terms $[(u\cdot\nabla)\boldsymbol{u}]^{n+\frac{1}{2}}_{i,j,k}$ have to be second order in time, and therefore the Taylor expansion in space and time is used. Derivatives in time are replaced by derivatives in space using the equation (3). Because of the staggered grid, we have to use different treatment of spacial discretization of advective terms. We define time centered values of velocity in cell centers (with integer indexes) and cell corners (with half indexes), so that

$$u^{n+\frac{1}{2},\mathrm{E}}_{i,j,k} = u^n_{i+\frac{1}{2},j,k} - \frac{\Delta x}{2}(u^n_x)_{i+\frac{1}{2},j,k} + \frac{\Delta t}{2}(u^n_t)_{i+\frac{1}{2},j,k}, \tag{8}$$

$$u^{n+\frac{1}{2},\mathrm{W}}_{i,j,k} = u^n_{i-\frac{1}{2},j,k} + \frac{\Delta x}{2}(u^n_x)_{i-\frac{1}{2},j,k} + \frac{\Delta t}{2}(u^n_t)_{i-\frac{1}{2},j,k}, \tag{9}$$

$$u^{n+\frac{1}{2},\mathrm{SB}}_{i+\frac{1}{2},j+\frac{1}{2},k+\frac{1}{2}} = u^n_{i+\frac{1}{2},j,k} + \frac{\Delta y}{2}(u^n_y)_{i+\frac{1}{2},j,k} + \frac{\Delta z}{2}(u^n_z)_{i+\frac{1}{2},j,k} + \frac{\Delta t}{2}(u^n_t)_{i+\frac{1}{2},j,k}, \quad (10)$$

$$u^{n+\frac{1}{2},\mathrm{NT}}_{i+\frac{1}{2},j+\frac{1}{2},k+\frac{1}{2}} = u^n_{i+\frac{1}{2},j+1,k+1} - \frac{\Delta y}{2}(u^n_y)_{i+\frac{1}{2},j+1,k+1} - \frac{\Delta z}{2}(u^n_z)_{i+\frac{1}{2},j+1,k+1} + \\ + \frac{\Delta t}{2}(u^n_t)_{i+\frac{1}{2},j+1,k+1}, \quad (11)$$

where W,E,S,N,B and T denote directions $-x$, $+x$, $-y$, $+y$, $-z$ and $+z$ respectively.

The spatial derivatives in eq. (8-11) are obtained using piecewise linear reconstruction in computational cells. Computed derivatives are then limited using a slope limiter

$$(u^n_x)^{\mathrm{L}}_{i+\frac{1}{2},j,k} = \frac{u^n_{i+\frac{1}{2}} - u^n_{i-\frac{1}{2}}}{\Delta x}, \quad (12)$$

$$(u^n_x)^{\mathrm{R}}_{i+\frac{1}{2},j,k} = \frac{u^n_{i+3/2} - u^n_{i+\frac{1}{2}}}{\Delta x}, \quad (13)$$

$$(u^n_x)_{i+\frac{1}{2},j,k} = \Gamma((u^n_x)^{\mathrm{L}}_{i+\frac{1}{2},j,k}, (u^n_x)^{\mathrm{R}}_{i+\frac{1}{2},j,k}), \quad (14)$$

where Γ is the slope limiter, that will be described later. The procedure is similar for other directions and velocity components.

The time derivatives in eq. (8-11) are expressed as

$$(u^n_t)_{i+\frac{1}{2},j,k} = \Delta_{i+\frac{1}{2},j,k}u^n - \nabla_{i+\frac{1}{2},j,k}p^n - (u_x)^n_{i+\frac{1}{2},j,k}u^n{}_{i+\frac{1}{2},j,k} - \quad (15)$$

$$-(\hat{u_y})^n_{i+\frac{1}{2},j,k}\bar{v}^n_{i+\frac{1}{2},j,k} - (\hat{u_z})^n_{i+\frac{1}{2},j,k}\bar{w}^n_{i+\frac{1}{2},j,k}, \quad (16)$$

where $\bar{v}$ and $\bar{w}$ are an averages of v and w in cells adjacent to $u_{i+\frac{1}{2},j,k}$

$$\bar{v}^n_{i+\frac{1}{2},j,k} = \frac{v^n_{i,j+\frac{1}{2},k} + v^n_{i+1,j+\frac{1}{2},k} + v^n_{i,j-\frac{1}{2},k} + v^n_{i+1,j-\frac{1}{2},k}}{4}, \quad (17)$$

and normal derivatives $\hat{u_{y,z}}$ are computed as:

if $v_{i+\frac{1}{2},j,k} \geq 0$

$$(\hat{u_y})^n_{i+\frac{1}{2},j,k} = \frac{u_{i+\frac{1}{2},j,k} - u_{i+\frac{1}{2},j-1,k}}{\Delta y} + \quad (18)$$

$$+\frac{1}{2}\left(1 - \frac{\bar{v}^n_{i+\frac{1}{2},j,k}\Delta t}{\Delta y}\right)\frac{(u^n_y)_{i+\frac{1}{2},j,k} - (u^n_y)_{i+\frac{1}{2},j-1,k}}{\Delta y}, \quad (19)$$

or if $v_{i+\frac{1}{2},j,k} \leq 0$

$$(\hat{u_y})^n_{i+\frac{1}{2},j,k} = \frac{u_{i+\frac{1}{2},j+1,k} - u_{i+\frac{1}{2},j,k}}{\Delta y} + \quad (20)$$

$$+\frac{1}{2}\left(1 - \frac{\bar{v}^n_{i+\frac{1}{2},j,k}\Delta t}{\Delta y}\right)\frac{(u^n_y)_{i+\frac{1}{2},j+1,k} - (u^n_y)_{i+\frac{1}{2},j,k}}{\Delta y}. \quad (21)$$

$$(22)$$

One unique value of $u_{i,j,k}$ and $u_{i+\frac{1}{2},j+\frac{1}{2},k+\frac{1}{2}}$ have to be obtained from reconstructed values from eq. (8-11). For cell centered values we used the same upwind procedure, as Tau [1994], while for

the corner values we used simple averaging in this version of the code

$$u_{i,j,k}^{n+\frac{1}{2}} = \begin{cases} u_{i,j,k}^{n+\frac{1}{2},\mathrm{W}} & \text{if } u_{i,j,k}^{n+\frac{1}{2},\mathrm{W}} \geq 0 \text{ and } u_{i,j,k}^{n+\frac{1}{2},\mathrm{W}} + u_{i,j,k}^{n+\frac{1}{2},\mathrm{E}} > 0, \\ 0 & \text{if } u_{i,j,k}^{n+\frac{1}{2},\mathrm{W}} < 0 \text{ and } u_{i,j,k}^{n+\frac{1}{2},\mathrm{E}} > 0, \\ u_{i,j,k}^{n+\frac{1}{2},\mathrm{E}} & \text{otherwise.} \end{cases}, \tag{23}$$

$$u_{i+\frac{1}{2},j+\frac{1}{2},k+\frac{1}{2}}^{n+\frac{1}{2}} = \frac{(u^{\mathrm{SW}} + u^{\mathrm{SE}} + u^{\mathrm{NW}} + u^{\mathrm{NE}})_{i+\frac{1}{2},j+\frac{1}{2},k+\frac{1}{2}}^{n+\frac{1}{2}}}{4}. \tag{24}$$

Finally, we can compute the advective terms in the equation (3) as

$$\begin{aligned} \left[u\frac{\partial u}{\partial x} + v\frac{\partial u}{\partial y} + w\frac{\partial u}{\partial z}\right]_{i+\frac{1}{2},j,k}^{n+\frac{1}{2}} &= \frac{u_{i+1,j,k}^{n+\frac{1}{2}} + u_{i,j,k}^{n+\frac{1}{2}}}{2}\frac{u_{i+1,j,k}^{n+\frac{1}{2}} - u_{i,j,k}^{n+\frac{1}{2}}}{\Delta x} \\ &+ \frac{v_{i+\frac{1}{2},j+\frac{1}{2},k+\frac{1}{2}}^{n+\frac{1}{2}} + v_{i+\frac{1}{2},j+\frac{1}{2},k-\frac{1}{2}}^{n+\frac{1}{2}} + v_{i+\frac{1}{2},j-\frac{1}{2},k+\frac{1}{2}}^{n+\frac{1}{2}} + v_{i+\frac{1}{2},j-\frac{1}{2},k-\frac{1}{2}}^{n+\frac{1}{2}}}{4} \cdot \\ &\cdot \frac{u_{i+\frac{1}{2},j+\frac{1}{2},k+\frac{1}{2}}^{n+\frac{1}{2}} + u_{i+\frac{1}{2},j+\frac{1}{2},k-\frac{1}{2}}^{n+\frac{1}{2}} - u_{i+\frac{1}{2},j-\frac{1}{2},k+\frac{1}{2}}^{n+\frac{1}{2}} - u_{i+\frac{1}{2},j-\frac{1}{2},k-\frac{1}{2}}^{n+\frac{1}{2}}}{\Delta y} \\ &+ \frac{w_{i+\frac{1}{2},j+\frac{1}{2},k+\frac{1}{2}}^{n+\frac{1}{2}} + w_{i+\frac{1}{2},j-\frac{1}{2},k+\frac{1}{2}}^{n+\frac{1}{2}} + w_{i+\frac{1}{2},j+\frac{1}{2},k-\frac{1}{2}}^{n+\frac{1}{2}} + w_{i+\frac{1}{2},j-\frac{1}{2},k-\frac{1}{2}}^{n+\frac{1}{2}}}{4} \cdot \\ &\cdot \frac{u_{i+\frac{1}{2},j+\frac{1}{2},k+\frac{1}{2}}^{n+\frac{1}{2}} + u_{i+\frac{1}{2},j-\frac{1}{2},k+\frac{1}{2}}^{n+\frac{1}{2}} - u_{i+\frac{1}{2},j+\frac{1}{2},k-\frac{1}{2}}^{n+\frac{1}{2}} - u_{i+\frac{1}{2},j-\frac{1}{2},k-\frac{1}{2}}^{n+\frac{1}{2}}}{\Delta z}. \end{aligned} \tag{25}$$

2.3 Slope limiters

Slope limiter $\Gamma(a,b))$ is a nonlinear function, that determinates the slope of reconstruction of a variable in the computation cell, in such a way, that no new extrema are produced. In this study we used following TVD limiters:

minmod	$\Gamma_{\mathrm{MM}}(a,b) = \begin{cases} \min(a,b) & \text{if } a>0 \wedge b>0, \\ \max(a,b) & \text{if } a<0 \wedge b<0, \\ 0 & \text{otherwise} \end{cases},$
generalised minmod	$\Gamma_{\mathrm{EMM}}(a,b) = \Gamma_{\mathrm{MM}}(\theta a, \theta b, \frac{a+b}{2}),$
van Albada	$\Gamma_{\mathrm{VA}} = b * \frac{r+r^2}{1+r^2},\ r = a/b,$
van Leer	$\Gamma_{\mathrm{VL}} = b * \frac{r+\lvert r\rvert}{1+r},\ r = a/b.$

For the extended minmod limiter we used the value $\theta = 2$, which is the maximum that holds the TVD property.

3 RESULTS

One of the most often computed cases of turbulent decaying flow is the Taylor-Green vortex. This flow is defined in a box of $(0, 2\pi)^3$ by initial conditions for the velocity in the form

$$u = \sin(x)\cos(y)\cos(z), \tag{26}$$

$$v = \cos(x)\sin(y)\cos(z), \tag{27}$$

$$w = 0, \tag{28}$$

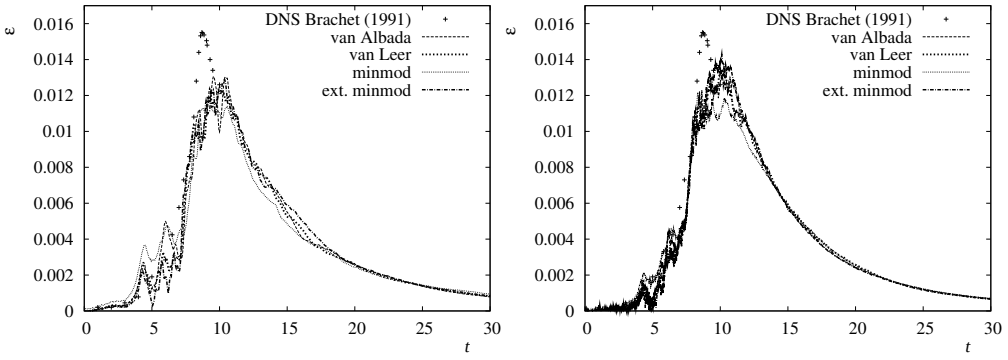

Figure 1: Plots of kinetic energy dissipation at resolution 64^3 (left) and 128^3 (right).

and by the pressure given by a solution of a pressure Poisson equation

$$p = p_0 + \frac{1}{16}(2 + \cos(2z))(\cos(2x) + \cos(2y)), \tag{29}$$

where p_0 is arbitrary (in the case of incompressible flow).

Taylor-Green vortex shows complex behaviour. At the beginning the flow is purely two-dimensional. The flow continues with forming of vortex sheets, breaking into smaller eddies, and after $t \approx 5$ the flow becomes turbulent. According to DNS of Brachet [1991] at $t \approx 9$ is the peak of the enstrophy and kinetic energy dissipation. After this peak the turbulent eddies dissipate in the self-similar energy cascade.

We performed our calculations on uniform grids with 64^3 and 128^3 cells.The molecular diffusion was set to a negligible value $\nu = 1/50000$, which results in the Reynolds number unresolvable exactly on current grids. Therefore numerical diffusion of the scheme had to act as an implicit subgrid stress model to transfer the energy to the unresolved scales of motion. For comparison we will use the DNS results of Brachet [1991] at $\mathrm{Re} = 5000$, that are very close to results at $\mathrm{Re} = 3000$ and therefore also close to the Reynolds number independence.

In figure 1 is plotted time history of kinetic energy dissipation, defined as

$$\varepsilon = -\frac{\mathrm{d}K}{\mathrm{d}t} = -\frac{\mathrm{d}}{\mathrm{d}t}\frac{\langle \|\boldsymbol{u}\|^2 \rangle}{2}, \tag{30}$$

scaled for direct comparison with Brachet [1991]. From the graph it is clear that the basic features of the time dependence are captured by the calculations. The 64^3 runs produced the broader and lower peak, than in 128^3. In both cases, however, the top of the main peak was lower, than in the DNS. This is in a good agreement with the ILES simulations in [Grinstein et al., 2007a]. The peak was also a little late. The differences between individual limiters are clearly visible, at least in 64^3 case. The most distinct one is the minmod limiter, which turns out to be overly diffusive. From the other limiters, extended minmod seems to produce result closest to the DNS. The time history of the kinetic energy K for the van Albada limiter (which is representative for the other) is depicted in figure 2. For a short time interval around $t = 10$ there can be found an area with scaling approximately $K \sim t^{-1.2}$, but for $t > 12$ there is a clear scaling $K \sim t^{-2}$. This is in agreement with Grinstein et al. [2007a], but our $t^{-1.2}$ interval seems to be too short.

At the time $t = 30$ we also computed the probability density functions (PDFs) of the velocity gradients and the pressure end the 3D kinetic energy spectra. In figure 3 are plotted examples of the PDFs for the extended minmod limiter (there were almost no visible differences between limiters).

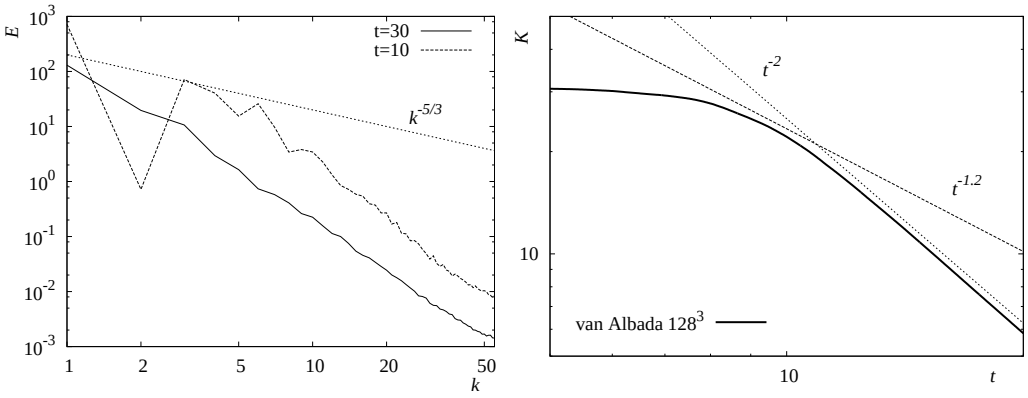

Figure 2: a) 3D spectra of kinetic energy and b) time history of total kinetic energy for van Albada limiter at resolution 128^3

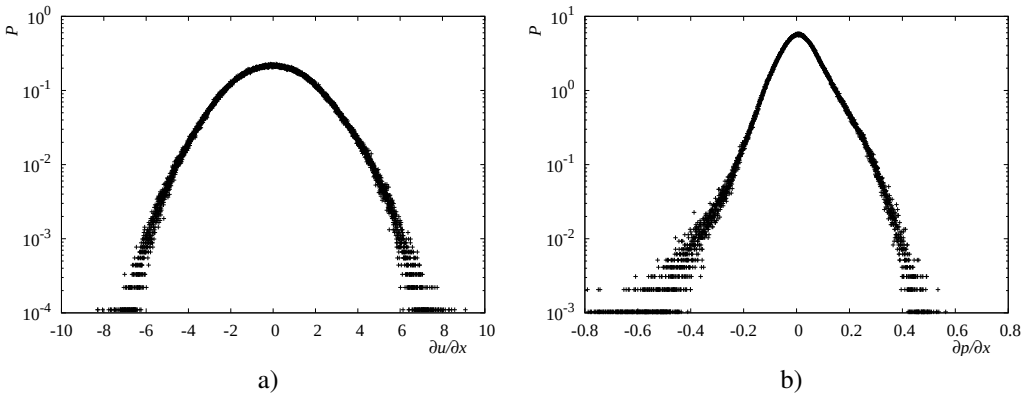

Figure 3: PDFs of a) $\frac{\partial u}{\partial x}$, b) $\frac{\partial p}{\partial x}$ for extended minmod limiter at resolution 128^3.

For both the velocity and the pressure the tails of the distributions show almost exponential nature as expected. However, the energy spectrum (for the van Albada limiter in figure 2) for $t = 10$ and $t = 30$ does not contain a clear inertial subrange with the Kolmogorov $k^{-5/3}$ power law. For $t = 30$ the spectrum scales as k^{-3} instead. All important wavenumbers are probably affected by the numerical dissipation of the scheme. Similar results were reported by Garnier et al. [1999].

In figure 4 are plotted isosurfaces of the pressure and the second largest eigenvalue of velocity gradient tensor [Jeog and Hussain, 1995]

$$\lambda_2 = \|\nabla \times \boldsymbol{u}\| - \sqrt{\|\nabla u\|^2 + \|\nabla v\|^2 + \|\nabla w\|^2}. \tag{31}$$

Both variables visualize vortex cores with pressure showing only the largest eddies and λ_2 more of the smaller eddies. Correlation between pressure lows and maxima of λ_2 is apparent.

4 CONCLUSIONS

We have developed a 3D model for incompressible flows using a projection method and a high-resolution method for the advective fluxes. We tested capability of this model for turbulent flow as an implicit large eddy simulation model using the Taylor-Green vortex. The model was capable to describe correctly many features of turbulent flow including the kinetic energy dissipation. One of

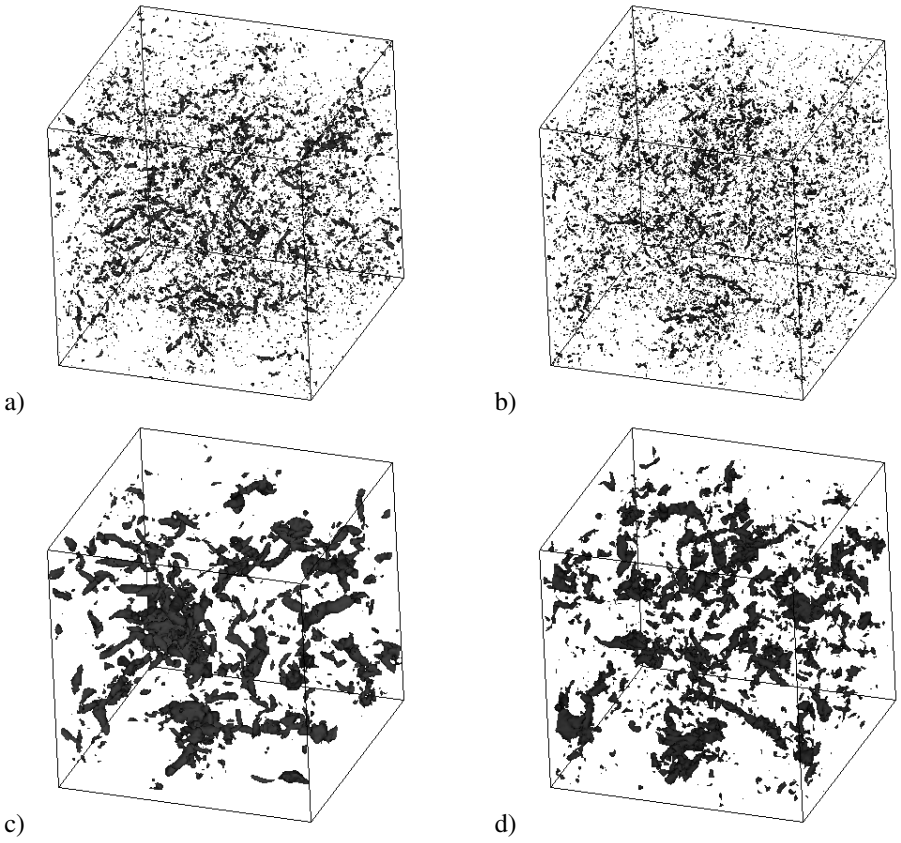

Figure 4: Volume renderings of a) λ_2 for minmod limiter, b) λ_2 for extended minmod limiter, c) pressure for minmod limiter, d) pressure for extended minmod limiter. All snapshots are at $t = 30$.

the remaining problems is the slope of the 3D energy spectrum, which does not contain well developed inertial subrange with $k^{-5/3}$ scaling. The development of the model will continue. We will try several other possibilities in the advective fluxes discretization (for example upwinding also in eq. (24). The next step will be simulations of wall bounded flows in a simple geometry (fully developed channel flow etc.). If the model will perform well we will continue with computations of separating flow, with the urban boundary layer as our main aim.

ACKNOWLEDGEMENTS

This research was supported by the Grant Agency of the Czech Academy of Sciences, grant no. T400300414, by the Grant Agency of the Czech Republic, grant no. 205/06/0727 and by the Czech Ministry of Education, Youth and Sports in the framework of the research plan MSM0021620860.

REFERENCES

Almgren, A., J. Bell, P. Colella, L. Howell, and M. Welcome. A conservative adaptive projection method for the variable density incompressible Navier-Stokes equations. *J. Comput. Phys.*, 142:1–46, 1998.

Almgren, A., J. Bell, and W. Szymczak. A numerical method for the incompressible navier-stokes equations based on an approximate projection. *SIAM J. Sci. Comput.*, 17:2, 1996.

Bell, J. B., P. Colella, and H. M. Glaz. A second-order projection method for the incompressible Navier-Stokes equations. *J. Comput. Phys.*, 85:257–283, 1989.

Bensow, R. E., M. G. Larson, and P. Vesterlund. Vorticity-strain residual-based turbulence modelling of the Taylor-Green vortex. *Internat. J. Numer. Methods Fluids*, 54:745–756, 2007.

Boris, J. P. and D. L. Book. Flux-corrected transport I. SHASTA, a fluid transport algorithm that works. *J. Comput. Phys.*, 135(2):172–186, 1997.

Brachet, M. E. Direct simulation of three-dimensional turbulence in the Taylor-Green vortex. *Fluid Dyn. Res.*, 8:1–8, 1991.

Brachet, M. E., D. I. Meiron, S. A. Orszag, B. G. Nickel, R. H. Morf, and U. Frisch. Small-scale structure of the Taylor-Green vortex. *J. Fluid Mech.*, 130:411–452, 1983.

Brown, D. L., R. Cortez, and M. L. Minion. Accurate projection methods for the incompressible Navier-Stokes equations. *J. Comput. Phys.*, 168:464–499, 2001.

Colella, P. and P. R. Woodward. The piecewise parabolic method (PPM) for gas-dynamical simulations. *J. Comput. Phys.*, 54:174–201, 1984.

Garnier, E., M. Mossi, P. Sagaut, P. Comte, and M. Deville. On the use of shock-capturing schemes for large-eddy simulation. *J. Comput. Phys.*, 153(2):273–311, 1999.

Grinstein, F., L. Margolin, and W. Rider. chapter Numerics for Iles, Limiting Algorithms. Cambridge University Press, Cambridge, 2007a.

Grinstein, F., L. Margolin, and W. Rider. *Implicit Large Eddy Simulation. Computing Turbulent Fluid Dynamics*. Cambridge University Press, Cambridge, 2007b.

Harten, A. High resolution schemes for hyperbolic conservation laws. *J. Comput. Phys.*, 49: 357–393, 1983.

Jameson, A., W. Schmidt, and E. Turkel. Numerical simulation of the euler equations by finite volume methods using Runge-Kutta time stepping schemes. In *AIAA 5th Computational Fluid Dynamics Conference (1981)*, pages AIAA Paper 81–1259, 1981.

Jeog, J. and F. Hussain. On the identification of a vortex. *J. Fluid Mech.*, 285:69–94, 1995.

Kim, J. and P. Moin. Application of a fractional-step method to incompressible Navier-Stokes equations. *J. Comput. Phys.*, 59:308–323, 1985.

Kolditz, O. *Computational Methods in Environmental Fluid Mechanics*. Springer, Berlin, 2002.

van Leer, B. Towards the ultimate conservative difference scheme V. a second-order sequel to Godunov's method. *J. Comput. Phys.*, 32:101–136, 1979.

Rider, W. Filtering non-solenoidal modes in numerical solutions of incompressible flows. *Internat. J. Numer. Methods Fluids*, 28:789–814, 1998.

Smolarkiewicz, P. K. and L. G. Margolin. MPDATA: a finite-difference solver for geophysical flows. *J. Comput. Phys.*, 140(2):459–480, 1998.

Smolarkiewicz, P. K., L. G. Margolin, and A. A. Wyszogrodzki. Implicit large-eddy simulation in meteorology: From boundary layers to climate. *J. of Fluid Eng.*, 129:1533–1539, 2007.

Tau, E. Y. A second-order projection method for the incompressible Navier-Stokes equations in arbitrary domains. *J. Comput. Phys.*, 115(1):147–152, 1994.